

Singlet-Triplet Physics and Shell Filling in Carbon Nanotube Double Quantum Dots

H. Ingerslev Jørgensen,^{1,2,*} K. Grove-Rasmussen,² K.-Y. Wang,¹
A. M. Blackburn,¹ K. Flensberg,² P. E. Lindelof,² and D. A. Williams¹

¹Hitachi Cambridge laboratory, Hitachi Europe Ltd., Cambridge CB3 0HE, United Kingdom

²Nano-Science Center, Niels Bohr Institute, University of Copenhagen,
Universitetsparken 5, DK-2100 Copenhagen Ø, Denmark

(Dated: November 11, 2021)

PACS numbers: 73.63.-b, 03.67.-Lx, 73.63.Fg, 73.63.Kv, 05.60.Gg

An artificial two-atomic molecule, also called a double quantum dot (DQD), is an ideal system for exploring few electron physics [1, 2, 3, 4, 5, 6, 7, 8, 9, 10, 11, 12, 13, 14]. Spin-entanglement between just two electrons can be explored in such systems where singlet and triplet states are accessible. These two spin-states can be regarded as the two states in a quantum two-state system, a so-called singlet-triplet qubit [15]. A very attractive material for realizing spin based qubits is the carbon nanotube (CNT) [16, 17, 18, 19, 20, 21], because it is expected to have a very long spin coherence time [10, 22, 23, 24, 25]. Here we show the existence of a gate-tunable singlet-triplet qubit in a CNT DQD. We show that the CNT DQD has clear shell structures of both four and eight electrons, with the singlet-triplet qubit present in the four-electron shells. We furthermore observe inelastic cotunneling via the singlet and triplet states, which we use to probe the splitting between singlet and triplet, in good agreement with theory.

Creating a qubit in a solid-state system demands control of the number of interacting electrons. This control has to date been obtained using semiconducting materials operated close to the band-gap edge. We show in this Letter that shell structures in CNT DQDs, owing to the 1-dimensional nature of the CNT, can be used to obtain the same kind of control. Both 4-electron and 8-electron (DQD)-shells are observed. We use one of the 4-electron shells to entangle the spin of two electrons and show that by separating the two electrons into separate QDs they form a spin triplet state, and by collecting them into the same QD they form a spin singlet state, i.e., a gate-tunable singlet-triplet qubit.

The device analyzed in this Letter, schematically shown in Fig. 1(a), is comprised of a CNT contacted by titanium electrodes, and gated by three top-gate electrodes, G1, CG (center-gate), and G2, made of aluminum oxide and titanium. The device has two strongly coupled quantum dots in series as confirmed by the observation of the so-called honeycomb pattern in current (I_{sd}) versus voltage applied to G1 (V_{G1}) and G2 (V_{G2}) (Fig. 1(b) and Fig. 2(a)) [5]. The tunneling barrier between the two dots is due to a defect in the CNT (similar to Ref. [17]). The resulting two dots have roughly equal charging energies and level spacings (see below), from which we infer that the defect is located under or close to the center

gate. The number of electrons in dot 1 and dot 2 can be controlled by tuning V_{G1} and V_{G2} , respectively. In the middle of each hexagon (white areas in Fig. 1(b) and Fig. 2(a)) a fixed number of electrons are localized in each dot, and electron transport is suppressed by Coulomb blockade. Along the entire edge of the hexagons (blue lines), single electron transport is allowed through molecular states formed in the DQD, indicating a strong coupling between the two dots. The height (width) of the hexagons corresponds to the energy required to add an extra electron in dot 1 (dot 2). In Fig.1(b) the width and height of the hexagons alternate in size in a regular pat-

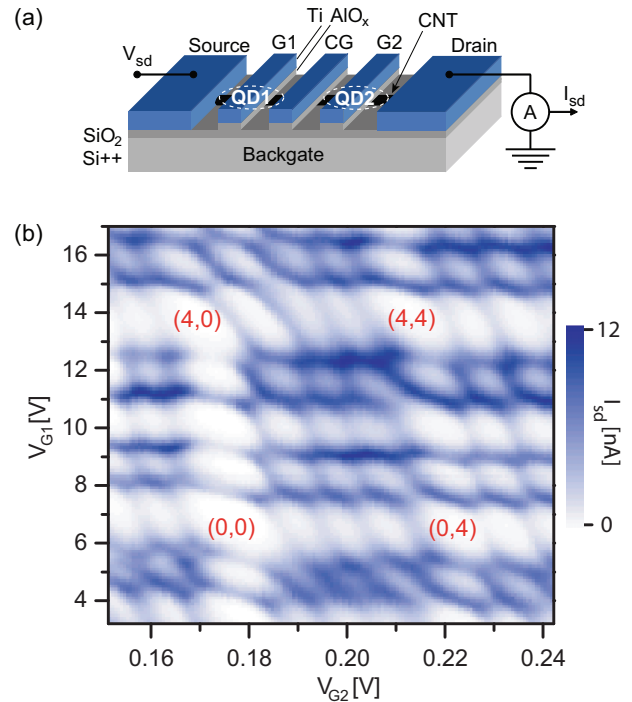


FIG. 1: **Shell filling of a carbon nanotube double quantum dot.** (a) Schematic figure of the device consisting of a carbon nanotube (CNT) contacted by titanium source and drain electrodes and gated with three top-gate electrodes, G1, CG (center gate), and G2. Two quantum dots (QD1, QD2) are formed in series, one under G1 and one under G2. (b) Surface plot of current (I_{sd}) at constant bias ($V_{sd} = 0.5$ mV) as function of voltage applied to G1 (V_{G1}) and G2 (V_{G2}). Red numbers (N,M) are shell occupation numbers for one 8-electron (DQD)-shell. Two further 8-electron shells were observed in connection the this shell, one below, and one to the right.

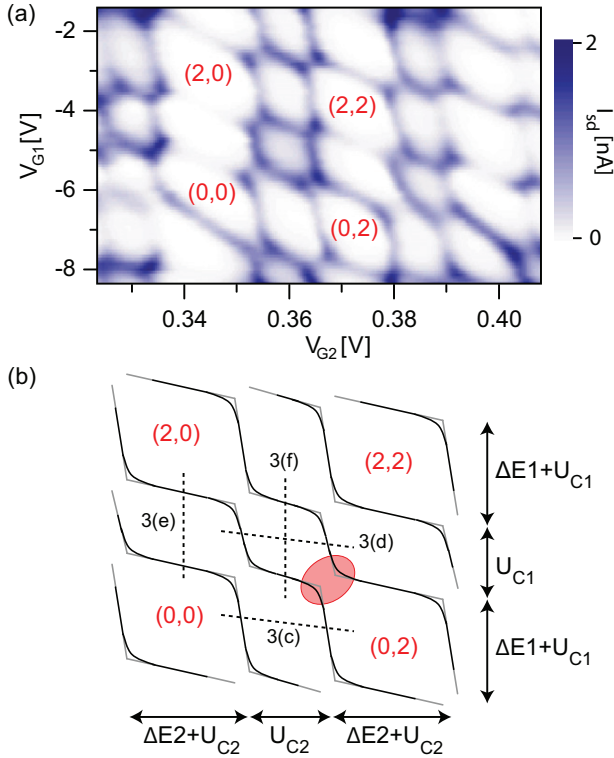


FIG. 2: **Four-electron DQD-shell structure.** (a) Surface plot of current (I_{sd}) at constant bias ($V_{sd} = 0.2$ mV) as function of voltage applied to G1 (V_{G1}) and G2 (V_{G2}). The numbers (N,M) are shell occupation numbers for one 4-electron shell. (b) Black lines: Schematic honeycomb diagram for a 4-electron shell with strong tunnel coupling, and a small cross capacitance. Gray lines: Same honeycomb diagram with negligible tunnel coupling. Dashed lines indicate where the line-traces in Fig. 3 are measured, and the red oval indicates the region analyzed in Fig. 4.

tern. The four hexagons marked with red numbers are distinctively larger than the other hexagons with three smaller hexagons in between, indicating that each dot has four-fold degenerate levels due to spin and orbital degeneracy [26, 27, 28]. An 8-electron shell structure of the DQD can therefore be identified in this plot. Shell occupation numbers (N,M), where N (M) is the level occupation number in dot 1 (dot 2) are written onto the honeycomb diagram.

The honeycomb diagram in Fig. 2(a) is measured for the same device but in another gate region where a new pattern in the sizes of the hexagons is observed. The hexagons alternate in size between large and small due to only spin degeneracy of the energy levels in each dot [26, 29], yielding a 4-electron shell structure of the DQD. The charging energies (U_{C1} , U_{C2}) and level spacings (ΔE_1 , ΔE_2) for the two dots can be extracted from the honeycomb pattern as schematically shown in Fig. 2(b). The gate coupling of G1 (G2) to dot 1 (dot 2) is found from bias spectroscopy plots (not shown), and we find $U_{C1} \sim 3$ meV and $\Delta E_1 \sim 1.2$ meV for dot 1, and $U_{C2} \sim 3.5$ meV and $\Delta E_2 \sim 1.5$ meV for dot 2. Since charging energy and level spacing are almost identical for the two dots we deduce that the two dots are roughly

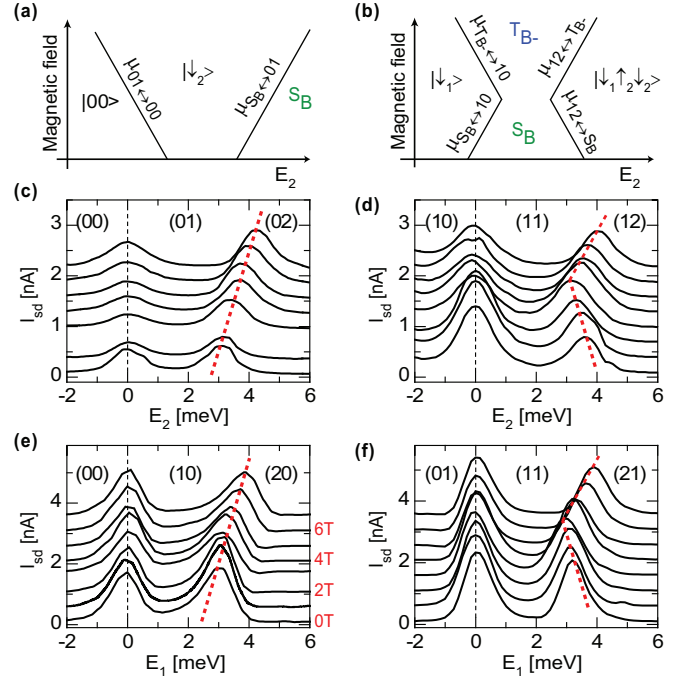


FIG. 3: **Singlet and Triplet states in a four-electron shell.** (a)-(b) Theoretical magnetic field dependence of the chemical potentials measured in (c)-(f). In (a) the 4-electron shell is filled from zero electrons ($|00\rangle$), to one spin-down electron in dot 2 ($|\downarrow_2\rangle$), to a singlet (S_B). In (b) the device is filled from a spin-down electron in dot 1 ($|\downarrow_1\rangle$), to either a singlet (S_B) or a triplet (T_{B-}) (see text), to a three particle state with one spin-down electron in dot 1 and both a spin-down and spin-up electron in dot 2 ($|\downarrow_1\uparrow_2\downarrow_2\rangle$). The line traces in (c)-(f) are extracted from honeycomb diagrams measured at $B = 0, 1, 2, \dots, 7$ T, where B is perpendicular to the nanotube. (c) and (e) Horizontal and vertical line traces through hexagon (0,1) and (1,0) as function of electrostatic potential in dot 2 (E_2) and dot 1 (E_1), respectively. (d) and (f) Horizontal and vertical line traces through hexagon (1,1). Each line in (c)-(f) is offset 0.2 nA, 0.3 nA, 0.3 nA, and 0.5 nA respectively for clarity, and the left-most peak is centered at zero.

equal in size. We have observed both 4-electron and 8-electron shell structures in two different devices.

We will in the rest of the Letter focus on a 4-electron shell with level spacings and charging energies similar to the 4-electron shell shown in Fig. 2(a), except $\Delta E_1 \sim 1.9$ meV. The singlet ground state between region (1,1) and (0,2) is in general a bonding state of the local singlet ($S(02)$, both electrons in dot 2), and the nonlocal singlet ($S(11)$, one electron in each dot):

$$S_B = \alpha S(11) + \beta S(02) \quad (1)$$

The detuning ($\varepsilon = E_2 - E_1$) dependent parameters α and β determine the weight of each state, and E_1 and E_2 are the electrostatic potentials in dot 1 and dot 2, respectively. Similarly for the triplets

$$\begin{aligned} T_{B-} &= \alpha' T_-(11) + \beta' T_-(02) \\ T_{B0} &= \alpha' T_0(11) + \beta' T_0(02) \\ T_{B+} &= \alpha' T_+(11) + \beta' T_+(02) \end{aligned} \quad (2)$$

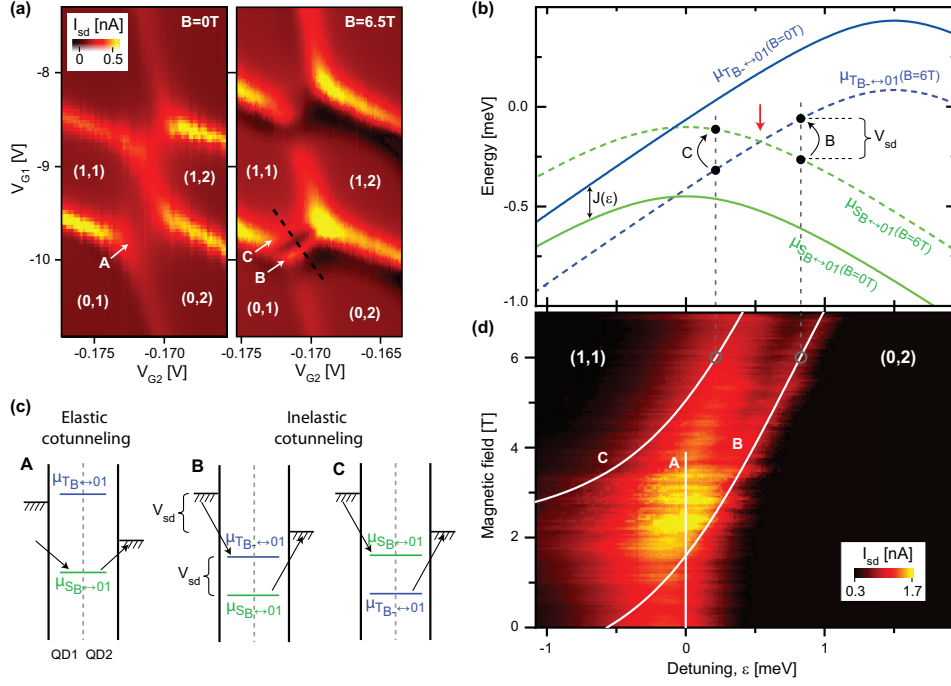


FIG. 4: **Singlet-triplet splitting probed by inelastic cotunneling.** (a) Small section of the honeycomb diagram analyzed in Fig. 3 with $V_{sd} = 50\mu V$ at $B = 0T$ (left) and $B = 6.5T$ (right). The numbers (N,M) indicate electron occupation of the 4-electron shell. (b) Chemical potentials for the singlet bonding ($\mu_{S_B \leftrightarrow 01}$) and triplet bonding ($\mu_{T_{B-} \leftrightarrow 01}$) with $B = 0T$ (solid green and blue lines) and with $B = 6T$ (dashed green and blue lines) calculated using Eq. (3) and (4). Onset of inelastic cotunneling which excites electrons from singlet to triplet (black arrow marked B) and from triplet to singlet (black arrow marked C) occurs when the separation between $\mu_{S_B \leftrightarrow 01}$ and $\mu_{T_{B-} \leftrightarrow 01}$ is equal to eV_{sd} . (c) Schematic transport diagrams for elastic cotunneling (A) and inelastic cotunneling (B and C). (d) Surface plot of current (I_{sd}) at $V_{sd} = 0.2mV$ versus magnetic field (B), and detuning (ϵ) along the black dashed line in (a). Onset of inelastic cotunneling occurs along the white lines marked B and C, calculated using Eq. (5) with $t = 0.32meV$, $\Delta E_2 = 1.5meV$, $V_{sd} = 0.2mV$, and $g = 2$. Dashed grey lines indicate where the two inelastic cotunneling processes shown in (b) occurs.

where $-, 0, +$ denotes the spin magnetic moment in the z -direction, $S_z = -1, 0, +1$. We will in the following show the existence of the singlet and triplet states, i.e., the singlet-triplet qubit, on the basis of a magnetic field spectroscopy on the 4-electron shell.

In Fig. 3(c) we analyze the magnetic field dependence of the width of hexagon (0,1), which involves 0, 1, and 2 electrons in dot 2. The chemical potential for these two Coulomb peaks is given by [13]: $\mu_{01 \leftrightarrow 00} \propto -\frac{1}{2}g\mu_B B$ and $\mu_{S_B \leftrightarrow 01} \propto +\frac{1}{2}g\mu_B B$, where $\mu_{01 \leftrightarrow 00}$ is the chemical potential for adding an electron to charge state (01) given no electron in the DQD-shell, and $\mu_{S_B \leftrightarrow 01}$ is the chemical potential for adding an electron in state S_B given one electron charge state (01). These two Coulomb peaks are therefore expected to separate by $g\mu_B B$ as shown in Fig. 3(a). The height of hexagon (1,0) are analogously expected to separate by $g\mu_B B$. The measurements in Fig. 3(c) and (e) are in good quantitative agreement with the theory in Fig. 3(a). The measured separation at 7 T is 0.95 meV and 0.8 meV in (c) and (e), respectively, where theory predicts $g\mu_B 7T = 0.81meV$ with $g = 2$ for nanotubes.

We now analyze the size of hexagon (1,1), which involves 1, 2, and 3 electrons in the DQD-shell. We show that by applying a magnetic field the 2-electron ground state can be changed from S_B to T_{B-} , which is used to

estimate the exchange energy (J) (energy separation between S_B and T_{B0}). Transport at the first Coulomb peak in Fig. 3(d) is through different chemical potentials at low and high magnetic field, given by [13] $\mu_{S_B \leftrightarrow 10} \propto +\frac{1}{2}g\mu_B B$ at low magnetic field ($g\mu_B B < J$), and $\mu_{T_{B-} \leftrightarrow 10} \propto -\frac{1}{2}g\mu_B B$ at high magnetic field ($g\mu_B B > J$). Similarly, transport at the second Coulomb peak in Fig. 3(d) is through $\mu_{12 \leftrightarrow S_B} \propto -\frac{1}{2}g\mu_B B$ at low magnetic field ($g\mu_B B < J$) and through $\mu_{12 \leftrightarrow T_{B-}} \propto +\frac{1}{2}g\mu_B B$ at high magnetic field ($g\mu_B B > J$) [13]. The same magnetic field dependence is expected for the height of hexagon (1,1) (see Fig. 3(f)). Therefore, for increasing magnetic field, hexagon (1,1) decreases in size when S_B is ground state, and increases in size when T_{B-} is ground state, schematically shown in Fig. 3(b). The measurements in Fig. 3(d) and (f) are in good agreement with the theory in Fig. 3(b) with the bend (shift of ground state from singlet to triplet) occurring at $B \sim 2 - 3T$, corresponding to an exchange energy of $J \sim 0.23 - 0.35meV$.

The exchange energy can, for large negative detuning (center of hexagon (1,1)), also be estimated from the tunnel coupling strength (t) using $J \simeq 4(t\sqrt{2})^2/U_{C1}$ (see supplement material) [13, 30]. We estimate $t \sim 0.32meV$ from the curvature of the hexagons at the anticrossings (see supplement material) [20]. This estimate of t yields a consistent estimate of the exchange energy

$J \simeq 4(t\sqrt{2})^2/U_{C1} \sim 0.27 \text{ meV}$.

The anticrossing between (1,1) and (0,2) (red area in fig. 2(b)) is analyzed in Fig. 4. We find that transport is governed by elastic and inelastic cotunneling via S_B and T_{B-} . The chemical potential for adding an electron to S_B and T_{B-} with $E_1 + E_2 = 0$, i.e., along the black dashed line in Fig. 4(a) is given by (see supplement):

$$\mu_{S_B \leftrightarrow 01}(\varepsilon, B) = -\frac{1}{2}\sqrt{(2t\sqrt{2})^2 + \varepsilon^2} + \frac{1}{2}g\mu_B B \quad (3)$$

$$\mu_{T_{B-} \leftrightarrow 01}(\varepsilon, B) = -\frac{1}{2}\left(\sqrt{(2t)^2 + (\varepsilon - \Delta E_2)^2} - \Delta E_2\right) - \frac{1}{2}g\mu_B B \quad (4)$$

We plot Eq. (3) and (4) in Fig. 4(b) with $B = 0 \text{ T}$ (solid green and blue lines), and with $B = 6 \text{ T}$ (dashed green and blue lines). We see that S_B is ground state for $B = 0 \text{ T}$, and that the two chemical potentials cross at elevated magnetic field, indicated with red arrow.

At low magnetic field one broad peak in conductance versus detuning between (1,1) and (0,2) is seen (Fig. 4(a), white arrow marked A). This conductance peak is due to elastic cotunneling via S_B , schematically shown in Fig. 4(c) (mark A). Since elastic cotunneling via S_B involves both $S(11)$ and $S(02)$, which have equal weight at $\varepsilon = 0$, the elastic cotunneling peak is centered around $\varepsilon = 0$. At high magnetic field the elastic cotunneling via S_B becomes suppressed because the ground state at $\varepsilon = 0$ changes from S_B to T_{B-} . Fig. 4(d) shows a surface plot of I_{sd} versus ε and B along the black dashed line in Fig. 4(a). The white vertical line marked A is the expected position of the elastic cotunneling.

At high magnetic field we observe two narrow peaks, marked B and C in Fig. 4(a). These two narrow peaks are due to the onset of inelastic cotunneling via S_B and T_{B-} , schematically shown in Fig. 4(c) mark B and C. Onset of inelastic cotunneling via S_B and T_{B-} occurs when the energy separation between their chemical potentials becomes equal to the applied bias:

$$eV_{sd} = \pm(\mu_{S_B \leftrightarrow 01}(\varepsilon, B) - \mu_{T_{B-} \leftrightarrow 01}(\varepsilon, B)) \quad (5)$$

We have from these two conditions calculated the onset of inelastic cotunneling in (ε, B) -space and plotted it as white lines marked B and C in Fig. 4(d). Note that no fitting parameters are used in Fig. 4(d), the parameters used, $t = 0.32 \text{ meV}$, $\Delta E_2 = 1.5 \text{ meV}$ were found in the analysis above.

METHODS

Fabrication and measurement setup

The devices are made on a highly doped silicon substrate with a top layer of silicon dioxide. The CNTs are grown by chemical vapor deposition from islands of catalyst material and subsequently contacted by 50 nm Titanium source and drain electrodes. Next, three narrow

top-gate electrodes are fabricated between the source and drain electrodes, consisting of aluminum oxide and titanium [16]. A schematic figure of the device together with the measurement setup is shown in Fig. 1(a). Source-drain voltage (V_{sd}) is applied to the source electrode and the drain electrode is connected through a current-to-voltage amplifier to ground. The three top-gate electrodes are named G1, CG (center gate), and G2 starting from the source electrode. For the device reported on in this Letter we saw that G1 had a much lower gate-coupling than G2 and CG (see Fig. 1(b) and Fig. 2(a)) which we attribute to the G1-electrode being damaged somewhere, weakening its gate-coupling. The gate coupling of G1 to dot 1 is $\alpha_{G1} = 2.9 \text{ meV/V}$, and gate coupling of G2 to dot 2 is $\alpha_{G2} = 400 \text{ meV/V}$. The center gate is kept at $V_{CG} = 0 \text{ V}$ for the measurements shown in this Letter. All data presented in this Letter are measured in a sorption pumped ^3He cryostat at 350 mK.

ACKNOWLEDGEMENTS

We wish to acknowledge the support of the EU-STREP ULTRA-1D program and the EU FP6 CANAPE project.

COMPETING FINANCIAL INTERESTS

The authors declare no competing financial interests.

* Electronic address: hij@fys.ku.dk

- [1] Petta, J. R., Johnson, A. C., Taylor, J. M., Laird, E. A., Jacoby, A., Lukin, M. D., Marcus, C. M., and Gossard, M. P. H. A. C. Coherent manipulation of coupled electron spins in semiconductor quantum dots. *Science* **309**, 2180 (2005).
- [2] Koppens, F. H. L., Folk, J. A., Elzerman, J. M., Hanson, R., van Beveren, L. H. W., Vink, I. T., Tranitz, H. P., Wegscheider, W., Kouwenhoven, L. P., and Vandersypen, L. M. K. Control and Detection of Singlet-Triplet Mixing in a Random Nuclear Field. *Science* **309**, 1346–1350 August (2005).
- [3] Johnson, A. C., Petta, J. R., Marcus, C. M., Hanson, M. P., and Gossard, A. C. Singlet-triplet spin blockade and charge sensing in a few-electron double quantum dot. *Phys. Rev. B* **72**(16), 165308 October (2005).
- [4] Johnson, A. C., Petta, J. R., Taylor, J. M., Yacoby, A., Lukin, M. D., Marcus, C. M., Hanson, M. P., and Gossard, A. C. Triplet-singlet spin relaxation via nuclei in a double quantum dot. *Nature (London)* **435**, 925–928 June (2005).
- [5] van der Wiel, W. G., de Franceschi, S., Elzerman, J. M., Fujisawa, T., Tarucha, S., and Kouwenhoven, L. P. Electron transport through double quantum dots. *Reviews of Modern Physics* **75**, 1–22 December (2002).
- [6] Pfund, A., Shorubalko, I., Ensslin, K., and Leturcq, R. Suppression of Spin Relaxation in an InAs Nanowire Double Quantum Dot. *Physical Review Letters* **99**(3), 036801 July (2007).
- [7] Ono, K., Austing, D. G., Tokura, Y., and Tarucha, S. Current Rectification by Pauli Exclusion in a Weakly

- Coupled Double Quantum Dot System. *Science* **297**, 1313–1317 August (2002).
- [8] Elzerman, J. M., Hanson, R., Greidanus, J. S., Willems van Beveren, L. H., de Franceschi, S., Vandersypen, L. M., Tarucha, S., and Kouwenhoven, L. P. Few-electron quantum dot circuit with integrated charge read out. *Phys. Rev. B* **67**(16), 161308 April (2003).
- [9] Fuhrer, A., Froberg, L. E., Pedersen, J. N., Larsson, M. W., Wacker, A., Pistol, M.-E., and Samuelson, L. Few Electron Double Quantum Dots in InAs/InP Nanowire Heterostructures. *NanoLetters* **7**(2), 243 February (2007).
- [10] Chan, V. C., Buehler, T. M., Ferguson, A. J., McCamey, D. R., Reilly, D. J., Dzurak, A. S., Clark, R. G., Yang, C., and Jamieson, D. N. Ion implanted Si:P double dot with gate tunable interdot coupling. *Journal of Applied Physics* **100**, 106104 November (2006).
- [11] Fasth, C., Fuhrer, A., Bjork, M. T., and Samuelson, L. Tunable Double Quantum Dots in InAs Nanowires Defined by Local Gate Electrodes. *NanoLetters* **5**(7), 1487 June (2005).
- [12] Hayashi, T., Fujisawa, T., Cheong, H. D., Jeong, Y. H., and Hirayama, Y. Coherent Manipulation of Electronic States in a Double Quantum Dot. *Physical Review Letters* **91**(22), 226804 November (2003).
- [13] Hanson, R., Kouwenhoven, L. P., Petta, J. R., Tarucha, S., and Vandersypen, L. M. K. Spins in few-electron quantum dots. *Reviews of Modern Physics* **79**, 1217–1265 October (2007).
- [14] Nowack, K. C., Koppens, F. H. L., Nazarov, Y. V., and Vandersypen, L. M. K. Coherent Control of a Single Electron Spin with Electric Fields. *Science Express* November (2007).
- [15] Nielsen, M. A. and Chuang, I. L. *Quantum Computation and Quantum Information*. Cambridge Univ. Press, Cambridge, ISBN, 0-521-63503-9 (2000).
- [16] Jørgensen, H. I., Grove-Rasmussen, K., Hauptmann, J. R., and Lindelof, P. E. Single wall carbon nanotube double quantum dot. *Applied Physics Letters* **89**, 2113 December (2006).
- [17] Mason, N., Biercuk, M. J., and Marcus, C. M. Local Gate Control of a Carbon Nanotube Double Quantum Dot. *Science* **303**, 655–658 January (2004).
- [18] Biercuk, M. J., Garaj, S., Mason, N., Chow, J. M., and Marcus, C. M. Gate-Defined Quantum Dots on Carbon Nanotubes. *Nano Lett.* **5**, 1267–1271 (2005).
- [19] Sappmaz, S., Meyer, C., Beliczynski, P., Jarillo-Herrero, P., and Kouwenhoven, L. P. Excited State Spectroscopy in Carbon Nanotube Double Quantum Dots. *Nano Lett.* **6**, 1350 (2006).
- [20] Gräber, M. R., Coish, W. A., Hoffmann, C., Weiss, M., Furer, J., Oberholzer, S., Loss, D., and Schönenberger, C. Molecular states in carbon nanotube double quantum dots. *Phys. Rev. B* **74**(7), 075427 August (2006).
- [21] Gräber, M. R., Weiss, M., and Schönenberger, C. Defining and controlling double quantum dots in single-walled carbon nanotubes. *Semiconductor Science Technology* **21**, 64 November (2006).
- [22] Gorman, J., Hasko, D. G., and Williams, D. A. Charge-Qubit Operation of an Isolated Double Quantum Dot. *Phys. Rev. Lett.* **95**(9), 090502 August (2005).
- [23] Cain, P. A., Ahmed, H., and Williams, D. A. Hole transport in coupled SiGe quantum dots for quantum computation. *Journal of Applied Physics* **92**, 346–350 July (2002).
- [24] Hu, Y., Churchill, H. H. O., Reilly, D. J., Xiang, J., Lieber, C. M., and Marcus, C. M. Double quantum dot with integrated charge sensor based on Ge/Si heterostructure nanowires. *ArXiv e-prints*, 0706.2271 **706** June (2007).
- [25] Coish, W. A. and Loss, D. Singlet-triplet decoherence due to nuclear spins in a double quantum dot. *Phys. Rev. B* **72**(12), 125337 September (2005).
- [26] Cobden, D. H. and Nygård, J. Shell Filling in Closed Single-Wall Carbon Nanotube Quantum Dots. *Phys. Rev. Lett.* **89**, 046803 (2002).
- [27] Moriyama, S., Fuse, T., Suzuki, M., Aoyagi, Y., and Ishibashi, K. Four-Electron Shell Structures and an Interacting Two-Electron System in Carbon-Nanotube Quantum Dots. *Physical Review Letters* **94**(18), 186806 May (2005).
- [28] Buitelaar, M. R., Bachtold, A., Nussbaumer, T., Iqbal, M., and Schönenberger, C. Multiwall Carbon Nanotubes as Quantum Dots. *Physical Review Letters* **88**(15), 156801 April (2002).
- [29] Moriyama, S., Fuse, T., Aoyagi, Y., and Ishibashi, K. Excitation spectroscopy of two-electron shell structures in carbon nanotube quantum dots in magnetic fields. *Applied Physics Letters* **87**, 073103 August (2005).
- [30] Loss, D. and Divincenzo, D. P. Quantum computation with quantum dots. *Phys. Rev. A* **57**, 120–126 January (1998).